

On the feasibility of studying the exospheres of Earth-like exoplanets by Lyman- α monitoring.

Detectability constraints for nearby M stars.

Ana I Gómez de Castro · Leire
Beitia-Antero · Sabina Ustamujic

Received: date / Accepted: date

Abstract Observations of the Earth's exosphere have unveiled an extended envelope of hydrogen reaching further than 10 Earth radii composed of atoms orbiting around the Earth. This large envelope increases significantly the opacity of the Earth to Lyman α ($\text{Ly}\alpha$) photons coming from the Sun, to the point of making feasible the detection of the Earth's transit signature from 1.35 pc if pointing with an 8 meter primary mirror space telescope through a clean line of sight ($N_H < 10^{17} \text{ cm}^{-2}$), as we show. In this work, we evaluate the potential detectability of Earth analogues orbiting around nearby M-type stars by monitoring the variability of the $\text{Ly}\alpha$ flux. We show that, in spite of the interstellar, heliospheric and astrospheric absorption, the transit signature in M5 V type stars would be detectable with a dedicated $\text{Ly}\alpha$ flux monitor implemented in a 4-8 m class space telescope. Such monitoring programs would enable measuring the robustness of planetary atmospheres under heavy space weather conditions like those produced by M-type stars. A 2-m class telescope, such as the World Space Observatory, would suffice to detect an Earth-like planet orbiting around Proxima Centauri, if there was such a planet or nearby M5 type stars.

This work has been funded by the Ministry of Economy and Competitiveness of Spain under grant numbers ESP2014-54243-R and ESP2015-68908-R

Ana I. Gómez de Castro
AEGORA Research Group, Universidad Complutense de Madrid, Plaza de Ciencias 3, 28040 Madrid, Spain
E-mail: aig@ucm.es

Leire Beitia-Antero
AEGORA Research Group, Universidad Complutense de Madrid, Plaza de Ciencias 3, 28040 Madrid, Spain

Sabina Ustamujic
AEGORA Research Group, Universidad Complutense de Madrid, Plaza de Ciencias 3, 28040 Madrid, Spain

Keywords ultraviolet: planetary systems; planets and satellites: atmospheres

1 Introduction

Atomic hydrogen is the dominant constituent of the upper terrestrial atmosphere. The primary source of atomic hydrogen is photodissociation by solar ultraviolet photons of molecular species (H_2O , CH_4 , H_2) originated in the troposphere that are transported to higher altitudes (Brasseur & Solomon 1996, Dessler et al. 1994). Above 90 km, in the thermosphere, direct production of atomic hydrogen is balanced by upward diffusion with an estimated total escape flux of $10^8 \text{ cm}^{-2} \text{ s}^{-1}$. This permanent loss of cold hydrogen atoms has a significant impact on long-term atmospheric evolution (Shizgal & Arkos, 1996).

Recent measurements have shown evidence of hot hydrogen atoms in the upper layers of the thermosphere. This population is generated by non-thermal processes and traces the coupling of the upper atmospheric layers to the plasmasphere, the magnetosphere and to space weather conditions in general (Qin & Waldrop, 2016). The interaction of hydrogen atoms with hot protons from the Solar wind and the energetic ions trapped in the ion belts lead to charge-exchange reactions and the production of energetic hydrogen atoms (1- 10^3 keV) that are key actors in the ion-neutral coupling between the atmosphere and magnetosphere. Hence, the precise determination of the atmospheric hydrogen distribution is vital for investigations of the chemistry and the thermal and particle flow in the Earth's atmosphere, as well as its coupling with Solar activity.

The distribution of exospheric hydrogen is studied through the Lyman α ($\text{Ly}\alpha$) transition, the most sensitive tracer to thin columns of neutral gas. Space probes have detected the $\text{Ly}\alpha$ photons from the Sun scattered by the hydrogen atoms in the Earth's exosphere. Missions such as the Magnetopause-to-Aurora Global Exploration (IMAGE) satellite (Fuselier et al. 2000) or the Two Wide-angle Imaging Neutral-atom Spectrometers (TWINS) (McComas et al. 2009) have carried out these measurements while navigating within the exosphere. From these observations we know that there exists an extended component of the exosphere, significantly stronger than predicted by the classical model (Chamberlain 1963). Extended exospheres have also been detected in Venus and Mars (Shizgal & Arkos, 1996) and it seems to be a common characteristic of terrestrial planets.

The detection of exoplanets has opened the possibility of studying planetary exospheres in other planetary systems submitted to diverse stellar radiation fields and space weather conditions. The transit of planetary exospheres in front of the stellar disk produces a net absorption that has been detected in the stellar $\text{Ly}\alpha$ profile. Since the seminal work by Vidal-Madjar et al. (2003) who detected the signature of HD 209458b exosphere, $\text{Ly}\alpha$ absorption has also been detected from the hot Jupiter HD 189733b (Lecavelier Des Etangs et al. 2010) and from the warm Neptune GJ 436b (Kulow et al. 2014, Ehrenreich et

al. 2015). However, it has not been detected in the two super-Earths observed to date, namely 55 Cnc e (Ehrenreich 2012) and HD 97658b (Bourrier et al. 2017). They have hypothesised that the lower extreme ultraviolet radiation from these stars diminishes the hydrogen production rate in the thermosphere and hence, the extent of the exosphere. In fact, it is possible that extended, Earth-like exospheres are not common or even detectable with the current techniques.

Measuring the impact of dramatic enhancement of the solar activity on planetary exospheres had been unthinkable until the detection of Earth-like exoplanets. These are orbiting around M dwarfs with strong magnetic fields and winds, thereby providing the ideal scenario to test Solar System-based planetary wind models under strong conditions. In this work, we evaluate the Earth's transmittance to solar Ly α photons and compute theoretical Ly α light curves for the transit of an Earth-like planet¹ orbiting around an M-dwarf star. We show that a 4-8 m class space telescope should be able to detect these variations provided the transit signature is not absorbed by the Interstellar Medium (ISM). In Section 2 the transmittance of the Earth exosphere to Ly α photons is evaluated. In Section 3 the light curves are computed for Earth-like planets orbiting some sample stars. The potential of Ly α monitoring for the study of planetary exospheres is discussed in Section 4. A brief summary is provided in Section 5.

2 Transmittance of the Earth's exosphere to Ly α photons

The GEO instrument (Mende et al. 2000) on board the IMAGE satellite found that the hydrogen density distribution is essentially cylindrically symmetric around the Sun-Earth line, exhibiting an enhancement in the antisolar direction, towards the geotail (Østgaard et al. 2003, hereafter O2003). Along any given solar zenithal angle, the density distribution is bimodal with a dominant central (or core) component and an extended component peaking at $\sim 8R_E$.

Later on, the TWINS mission obtained the 3D distribution of H I atoms between $3R_E$ and $8R_E$ and reported enhancements by a factor of $\sim 2 - 3$ of the extended component with respect to O2003 (Zoennchen et al. 2010).

From these works, the distribution of hydrogen in the Earth's exosphere can be modelled as,

$$n_H(r) = n_0 e^{-\frac{r}{r_0}} + \kappa n_1 e^{-\frac{r}{r_1}} \quad (1)$$

for any given solar-zenital angle. r is the radial distance to the center of the Earth, (n_0, r_0) are the density and characteristic radius of the core component, dominated by the Earth photoevaporative flow, and (n_1, r_1) are the density and characteristic radius of the extended component. κ is a coefficient introduced to modify at will the relative strength of the extended component

¹ An 'Earth-like' planet is assumed to have the same extended exosphere as the Earth's.

with respect to the core component. Minimum values of these coefficients are: $n_0 = 10^4 \text{ cm}^{-3}$, $n_1 = 7 \text{ cm}^{-3}$, $r_0 = 1.02R_E$, $r_1 = 8.2R_E$ and $\kappa = 1$ (O2003).

Using this distribution as a baseline, the column density of exospheric hydrogen (N_H) and the transmittance of the Earth's exosphere to stellar Ly α photons for a distant observer located on the plane of the ecliptic can be directly worked out. At a given projected distance, R , from the center of the Earth, the stellar Ly α photons propagate through a layer of thickness $2z_l = 2(r_e^2 - R^2)^{1/2}$, with r_e the radius of the exosphere taken to be $15 R_E$ for this calculation. The output radiation, $I(R)$, can be calculated from the standard radiation transfer equation,

$$\frac{dI}{I} = -\sigma n(r) dz, \quad (2)$$

being $z = \sqrt{r^2 - R^2}$ the depth of gas layer through which the Ly α radiation is being transferred and $\sigma = 5.9 \times 10^{-12} \times 1050^{-1/2} \text{ cm}^2$ (Bishop, 1999) the cross section of hydrogen to Ly α radiation; 1050 K is the reference temperature of the exospheric hydrogen (Bishop 1999, O2003).

This equation can be numerically integrated and for $dz \ll \sigma n(r)$ takes the form,

$$4\pi I(R) = \int_{-z_l}^{+z_l} I_0 \sigma n(r) dz \quad (3)$$

The transmittance of the Earth's exosphere at a given projected distance is defined as,

$$Tr(R) = \frac{I(R)}{I_0} \quad (4)$$

and it is plotted in Fig. 1 for various possible $n(r)$ distributions; the reference curve is based on IMAGE/GEO results (O2003). We observe that at distances $> 3 - 4R_E$, the transmittance is very sensitive to the strength of the extended component. Additional transmittance curves enhancing the strength of the extended component by a factor of $\kappa = 5$ to 40 with respect to O2003 are also represented; $\kappa = 5$ mimics well the results from TWINS (Zoennchen et al. 2010).

2.1 The impact of the ISM on the observability

During transit observations, the exospheric Ly α absorption is expected to be maximum at the core of the stellar Ly α profile. Unfortunately, the radial velocity of the nearby M type stars is similar to that of the local clouds in the ISM which absorb efficiently the core of the line (see *e.g.* Youngblood et al. 2016). As a result, though large Earth-like exospheres may produce a measurable signature during transit in the Ly α light curves (see below), this would pass unnoticed if the core of the line is fully absorbed by the ISM; a

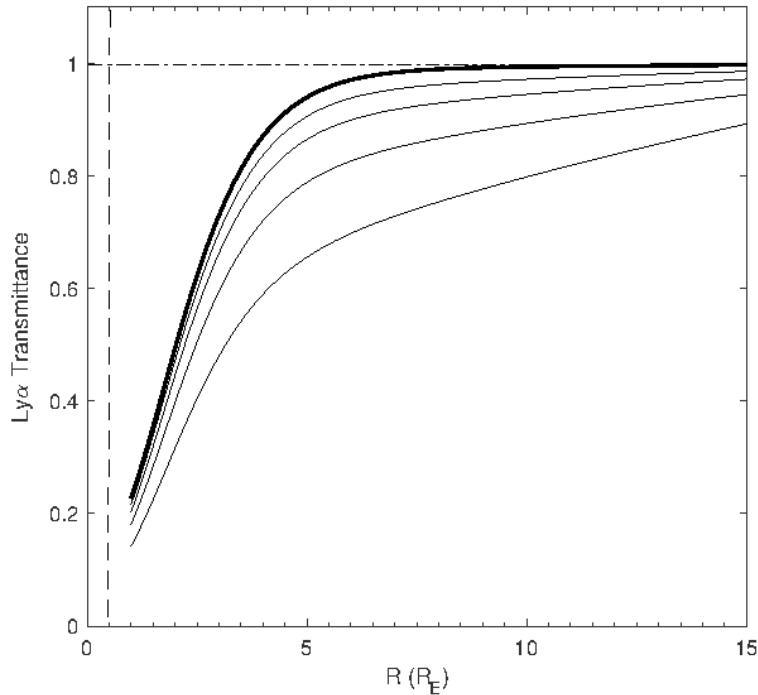


Fig. 1 Transmittance of the Earth’s exosphere to Ly α photons in normal incidence from the Sun as a function of the radial distance to the center of the Earth (units: Earth radii (R_E)). κ indicates the relative strength of the extended component with respect to the baseline model obtained from IMAGE/GEO data (O2003). $\kappa = 1$ corresponds to the baseline model (bold). Incremental κ values: 5, 10, 20, 40 are represented with thin lines. Measurements based on TWINS suggest $\kappa = 5$ (Zoennchen et al. 2010). The geometric cross-section of the solid Earth to solar Ly α photons is represented for guidance (dashed line).

hydrogen column of $N_H \simeq 5 \times 10^{17} \text{ cm}^{-2}$ suffices to block the Ly α flux (see *e.g.* Gómez de Castro et al. 2016).

The lines of sight with measured Ly α absorption are plotted in Figure 2 from the compilations by Wood et al. 2005 and Redfield and Linsky 2008. The location of the Local Interstellar Cloud (LIC) is neatly traced. Additional clouds and filaments are also identified. The distribution in the sky of the local Ly α absorbers is compared with the distribution of M stars in the northern hemisphere as compiled for the CARMENES input catalogue² (Alonso-Floriano et al. 2015). Figure 2 also shows that the information on the

² CARMENES is conducting a 600-night exoplanet survey targeting 300 M dwarfs during Guaranteed Time Observations. The main scientific objective of CARMENES is to carry out a survey of late-type main sequence stars with the goal of detecting low-mass planets in their habitable zones. In the focus of the project are very cool dwarf stars later than spectral type M4 and moderately active stars.

characteristics and spatial distribution of the local Ly α absorbers is rather scarce.

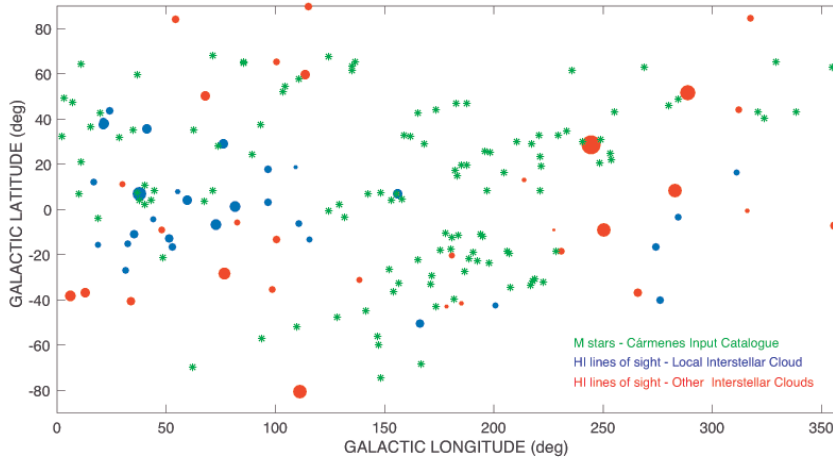


Fig. 2 Distribution in the sky of the Ly α absorbers as per works by Wood et al. 2005 and Redfield and Linsky 2008 compared with the location of the M-type stars in the CARMENES input catalogue (marked with star symbols). Absorbers are marked with dots. The size of dots scales with the HI column density (N_H), from $N_H = 10^{17.2} \text{ cm}^{-2}$ for the smallest dots to $N_H = 10^{18.6} \text{ cm}^{-2}$ for the largest ones.

The existence of diffuse clouds in the ISM however, has not prevented the detection of hot Jupiters transits (see *e.g.* Vidal-Madjar et al. 2003) because exospheres are heated by the stellar XUV radiation fields³ and disturbed by the interaction with the stellar wind. The XUV flux is efficiently absorbed by the upper atmospheric layers and heats the gas favouring the thermal escape. As a result, a significant fraction of the exospheric hydrogen may reach velocities high enough to allow the detection in spite of the ISM absorption of the line core. The high optical depth of the Ly α line also assists the detection of the feature since the lowermost exospheric layers saturate the core of the Ly α profile and produce extended wings.

To evaluate the impact of high stellar XUV fluxes on the dynamics of Earth-like planets' exospheres we have resourced to the models developed by Erkaev et al. (2013); these authors analysed the atmospheric escape by solving the equations of a hydrodynamical flow including the volume heating rates by stellar soft X-ray and UV radiation. Outputs from the model are the density ($n(r)$), temperature ($T(r)$) and expansion velocity ($V_e(r)$) from the thermosphere to the outer exosphere. Models are calculated for a broad range of XUV fluxes, spanning from the level of the quiet Sun (XUV_{\odot}) to 100 times this value⁴. For instance, the XUV fluxes irradiating the exoplanets GJ 436b

³ XUV stands for X-ray and extreme UV photons.

⁴ The solar XUV flux at 1 AU is $XUV_{\odot} = 4.64 \text{ erg cm}^{-2} \text{ s}^{-1}$ (Ribas et al., 2005).

and GJ 674b are $355 \text{ erg cm}^{-2} \text{ s}^{-1}$ (76 XUV_{\odot}) and $3631 \text{ erg cm}^{-2} \text{ s}^{-1}$ (783 XUV_{\odot}) respectively (Sanz-Forcada et al. 2011). Both GJ 436 and GJ 674 are M2.5 V stars. Recently, France et al. (2016) have derived an XUV flux of $10 - 70 \text{ cm}^{-2} \text{ s}^{-1}$ in the habitable zone of typical exoplanet host stars.

Using as input the functions $n(r)$, $T(r)$ and $V_e(r)$ from Erkaev et al. 2013, we have computed the optical depth of the exospheric absorption of Ly α photons as a function of R , the cylindrical distance to the center of the Earth-like planet and the velocity of the exospheric gas v , as,

$$\tau(R, v) = \sigma \int_{-z_t}^{+z_t} n(r) f(r, v) dz \quad (5)$$

with $f(v, z)$ the normalized velocity profile of the gas at a distance r obtained by the convolution of the thermal broadening (assuming $T(r)$ as in Erkaev et al. 2013) and the natural broadening profile ($\phi(v)$). Hence,

$$f(r, v) = \frac{\exp(-U(r, v))}{2kT(r)/m_H} * \phi(v) \quad (6)$$

and,

$$U(r, v) = \frac{(v - V_e(r))^2}{2kT(r)/m_H} \quad (7)$$

Note that m_H is the mass of a hydrogen atom, k is the Boltzmann constant and

$$r = \sqrt{(R^2 + z^2)} \quad (8)$$

The transmittance is computed as per Eq. 4. As shown in Figure 3, the exospheric transmittance displays a strengthening of the blue shifted wing as both the stellar XUV flux and the escape flow increase. Also, the high optical depth of the Ly α line produces broad wings that result on a 33% of the transmittance occurring at Doppler shifts larger than $\pm 40 \text{ km s}^{-1}$ for an XUV flux equal to XUV_{\odot} (this value raises to a 58% for a XUV flux = 50 XUV_{\odot}). Therefore, the detectability is strongly dependent on the XUV flux. Stable exospheres are more difficult to detect than unstable, photoevaporating exospheres forced by the action of a strong stellar XUV radiation field. Note that the high XUV radiation from M-type stars may result in the full evaporation of the planetary exosphere/atmosphere rendering fruitless any atmospheric research on these sources. Otherwise, the investigation of the atmospheres stability under heavy XUV irradiation is a fundamental for planetary/exoplanetary research.

Detectability also depends on the properties of the individual sources, Ly α profile, ISM absorption, and radial velocity as illustrated in Fig. 4, where synthetic profiles are represented for the transit of an Earth-like exoplanet orbiting in the habitable zone around M5 and M0 V stars. For the sake of the calculation, we have selected two nearby M stars with well measured Ly α fluxes, namely AU Mic (M0 V) and Proxima Centauri (M5.5 V) (see Table 1). In all cases, an Earth-like planet is assumed to be orbiting in the habitable zone. The stellar Ly α profiles have been taken from Wood et al. (2001, 2005) who reconstructed the stellar Ly α emission after removing the effect of the

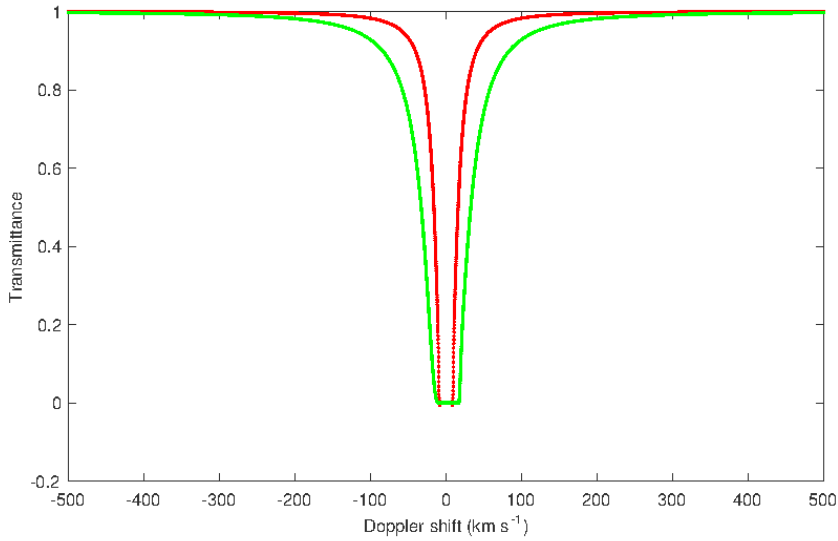


Fig. 3 Transmittance of the atmosphere of an Earth-like planet to stellar $\text{Ly}\alpha$ photons as a function of the Doppler shift with respect to $\text{Ly}\alpha$ rest wavelength. Atmospheric models come from Erkaev et al. 2013. The red line represents the transmittance of an exosphere irradiated with an XUV flux alike the produced by the quiet Sun. The green line also represents the transmittance but assuming an XUV flux 50 times higher.

ISM absorption for a large set of cool stars. In particular, the AU Mic profile and the Proxima Cen profile have selected to represent M0 and M5 stars. In a first step, the absorption produced by the exosphere of the transiting planet is computed as per the procedure defined in Eq. 3-8. In a second step, this output profile is assumed to cross an interstellar cloud with column density, $N_H = 10^{18} \text{ cm}^{-2}$, temperature, $T = 8,000 \text{ K}$ and radial velocity with respect to the star, $\Delta V = 0, 15$ and 30 km s^{-1} to evaluate the impact of the relative velocity between the cloud and the star in the detectability. As expected, the transit signal increases as the stellar radius decreases and becomes comparable to the size of the Earth exosphere.

In summary, the detectability of $\text{Ly}\alpha$ transits of Earth-like exoplanets orbiting M-type stars will depend strongly on the stellar spectral type (stellar radius), the XUV flux that drives the atmospheric outflows and the chance of observing along clean lines of sight. Planets orbiting around high velocity stars, such as the Kaptein star, will also offer a good chance for exospheric studies since most of the local ISM clouds have radial velocities about 10-40 km/s.

Table 1 Parameters used for the transit calculation.

Parameter	AU Mic	Prox Cen
Spectral Type ^(a)	M0V	M5.5V
Radius (R_{\odot})	0.5 ^(b)	0.14 ^(c)
Mass (M_{\odot})	0.6 ^(d)	0.12 ^(e)
Semimajor axis of the orbit (a.u.)	0.3	0.032
$F_{Ly\alpha}^0$ (10^{-12} erg cm $^{-2}$ s $^{-1}$) ^(a)	10.3	4.21
$F_{Ly\alpha}$ (10^{-12} erg cm $^{-2}$ s $^{-1}$) ^(a)	2	1.2
$\log N_H$ (cm $^{-2}$) ^(a)	17.6	18.36
d (pc) ^(a)	9.9	1.30

$F_{Ly\alpha}^0$ is the stellar Ly α flux reconstructed by Wood et al. 2005.

$F_{Ly\alpha}$ is the observed Ly α flux calculated from Hubble archival data.

References: (a) Wood et al. 2005; (b) Rhee et al. 2007;

(c) Maldonado et al. 2015; (d) Chen et al. 2005;

(e) Benedict et al. 2016.

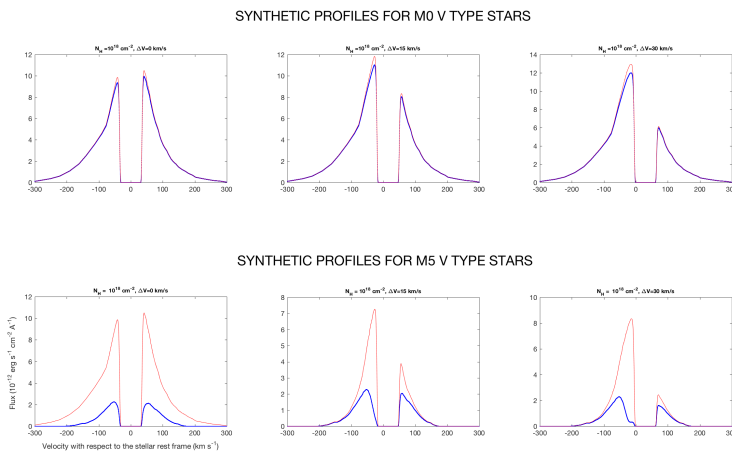


Fig. 4 Simulated Ly α profiles for M0 and M5 spectral type stars. The Ly α profile in the absence of a transiting planet is plotted in red. The blue-solid line represents the profile during transit (at maximum). In all cases, it is assumed that there is an ISM cloud in the line of sight with $N_H = 10^{18}$ cm $^{-2}$ and $T = 8,000$ K. The relative velocity between the cloud and the star is taken to be 0, 15 and 30 km s $^{-1}$ in the left, central and right panels.

3 Calculation of the transit light curves for some sample stars

Earth-like planets are being detected by the transit method: orbiting planets occult the stellar radiation when crossing the line of sight, producing a measurable variation of the radiation that reaches the observer. The best suited stars for this purpose are M-dwarfs. They are the smallest and the most common class of stars in the Galaxy. GJ 1132b (Berta-Thompson et al. 2015), Kepler-42c (Borucki et al. 2011), GJ 3470b (Bonfils et al. 2012) or Kepler-1646b (Morton et al. 2016) are some examples of positive detections of exo-

planets around M stars. A candidate to Earth-like planet has been detected in Proxima Centauri, at 1.3 pc from the Sun (Anglada-Escudé, 2016). Earth-like exoplanets have also been detected around earlier types of cool stars such as Kepler-78b (Pepe et al. 2013), a K-type dwarf, or the late G-type star Kepler-93b (Dressing & Charbonneau 2015).

We have computed transit light curves for AU Mic and Proxima Cen using the parameters in Table 1. In addition, we have computed the light curve for α -Cen, the nearest analogue to the Sun, to evaluate the detectability of the Earth exosphere from a distance of 1.3 pc. The Sun and α -Cen have similar Ly α fluxes and the Ly α absorption along the line of sight is well quantified (Wood et al. 2005). From the data available in the Hubble archive, we have measured the observed Ly α flux of α -Cen to be 4.2×10^{-11} erg cm $^{-2}$ s $^{-1}$. Note that the Ly α flux varies within the activity cycle. During the solar cycle, the Ly α irradiance varies⁵ roughly between 3.5 and 6.5×10^{11} photons cm $^{-2}$ s $^{-1}$ (Rairden et al. 1986). The flux used for our calculations is similar to that of the active Sun observed from α -Cen.

For all the calculations, the Ly α emissivity has been taken as constant over the stellar disk; the presence of dark spots and active regions has been neglected though the light curves could also be used to detect them. In all cases, the inclination is assumed to be 90° (edge-on).

The light curves have been calculated under the assumption that impact of the ISM blockage of the transit signature is equivalent to degrading the exosphere transmittance to a 10% of the original value. According to Fig. 4 this is a reasonable approach for atmospheres illuminated by high XUV fluxes. The theoretical light curves are shown Fig. 5. The light curve varies from source to source due to differences in the stellar radius, transit duration and location of the habitable zone (see Table 1).

3.1 Detectability

To evaluate the feasibility of detecting the light curves in Fig. 5, an instrumental set-up needs to be defined. We have assumed a rather simple configuration consisting of a Ly α monitor operating in a 4 m primary mirror space telescope. The monitor is a low dispersion slitless spectrograph with resolving power 800 serviced by a photon counting CsI MCP detector; this configuration is similar to the implemented in the Focal Camera Unit (FCU) of the WSO-UV mission (see Sachkov et al 2016 for details). A spectrograph is implemented instead of a Ly α filter because it is the most efficient from the radiometric point of view (see, e.g. Gómez de Castro et al. 2014). The light path to the detector includes three reflections (primary, secondary and pick-off mirror) each with high reflectivity (80%) and the low dispersion grating with reflectivity 20% at 122 nm. A 20% detector quantum efficiency at 122 nm has been considered (Vallerga et al. 2009). For the sake of the simulation, we have assumed a stable

⁵ <https://lasp.colorado.edu/lisirg/lya>

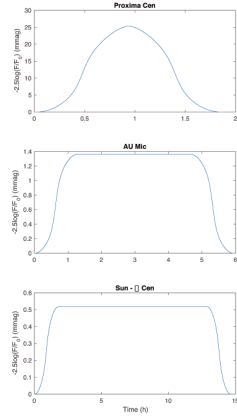


Fig. 5 Theoretical Ly α light curves from the transit model for Proxima Cen, AU Mic and α Cen assuming that 90% of the transit signal is absorbed by the ISM (see text).

heliospheric background and have neglected the geocoronal emission. The heliospheric background is taken to be 5.5×10^{-3} photons $cm^{-2}s^{-1}$ (Lallement et al. 1996, Koutroumpa et al. 2017).

Note that the Earth geocoronal emission has been neglected because the observation is assumed to be carried out from a space telescope in geosynchronous orbit such as the WSO-UV or above. During the observation the satellite is assumed to be far from the magnetotail and pointing in the anti-Earth direction⁶

With these provisions, the SNR is given by,

$$SNR = \frac{\Delta SCR \times T_{\text{exp}}}{\sqrt{SCR \times T_{\text{exp}} + N_{\text{pix}} \times BCR \times T_{\text{exp}}}} \quad (10)$$

with

- SCR , the stellar Ly α count rate.
- BCR , the Ly α background count rate.

⁶ This is the optimal configuration: the space telescope observes the target when it is at opposition with respect to the Earth. This orientation minimizes the geocoronal Ly α background since most of the hydrogen atoms are located close to the base of the exosphere. Along a given line of sight, the contribution of the Earth geocorona to the Ly α flux is given by,

$$F_{Ly\alpha} = \int_{r_0}^{\infty} I_{Ly\alpha} dr \quad (9)$$

According to O2003, the geocorona Ly α intensity follows the law: $I_{Ly\alpha} = 18.1 \exp(-r/1.01R_E) + 1.05 \exp(-r/8.21R_E)$ with $I_{Ly\alpha}$ in kilo Rayleighs (kR). At low Earth orbit (LEO), $r_0 \simeq 6750$ km, $F_{Ly\alpha}(\text{LEO}) = 6.77$ kR while in a geosynchronous orbit, $r_0 = 6.6R_E$, $F_{Ly\alpha}(\text{GO}) = 0.08$ kR. Thus the contribution is significantly smaller and lower than the heliospheric background (Lallement et al. 1996, Koutroumpa et al. 2017).

- ΔSCR measures the depth of transit: the out of transit SCR minus the SCR at maximum depth during transit.
- N_{pix} the number of pixels used to integrate the signal. For this calculation, $N_{pix} = 4$ is assumed.

The count rate is derived from the Ly α flux, $F_{Ly\alpha}$, from the usual expression:

$$SCR = \left(\frac{D}{4m}\right)^2 A_{eff} \frac{F_{Ly\alpha}}{h\nu_{Ly\alpha}} \quad (11)$$

with A_{eff} the effective area,

$$A_{eff} = \pi \left(\frac{400}{2}\right)^2 0.8^3 0.2^2 = 2.6 \times 10^3 \text{cm}^2 \quad (12)$$

and $(D/4m)$ a scale factor to increase the effective area with the size (D) of the primary mirror of the telescope.

SNRs have been computed neglecting the ISM blockage of the transit signature because its impact in the light curve depends on many factors⁷ that depend on the particular source under study. To increase the SNR, the counts have been binned into time steps of 2, 4 and 10 minutes for Proxima Centauri, AU Mic and α Cen, respectively. With these provisions the SNR reached is: 11.7, 1.2 and 1.5 for Proxima Centauri, AU Mic and α Cen, respectively. If the size of the primary mirror is increased to 12 m ($D/4m = 3$), the SNR rises to 3.5 for AU Mic and to 4.4 for α Cen; see the light curves in Fig. 6.

Note that the presence of ISM absorption can be directly accounted in ΔSCR . For instance, the presence of a Ly α absorber with $N_H = 10^{18} \text{cm}^{-2}$ and $T = 8,000 \text{K}$ in the line of sight to an M0 V star decreases ΔSCR by a 96.5-97.5 % in the range of relative velocities used for the simulated profiles in Fig. 4. However, the same absorber in the line of sight to an M5 V star decreases ΔSCR by barely a factor of 2 (43.8-60.2 % depending on the cloud velocity). In all cases, the total counts can be raised by co-adding several observations of the transit to reach SNR values similar to those quoted above for the non-ISM absorption case. This technique is performed routinely by missions, such as Kepler, devoted to exoplanetary research.

4 Discussion: Potential exoplanetary studies using a Ly α monitor

In Sect. 2 and 3.1, we have shown that extended, Earth-like exospheres produce detectable absorption signature over the stellar Ly α emission because of the strong opacity of the line and the large extent of the Earth's exosphere. This signature is especially strong in small stars such as the M dwarfs. So far, Ly α

⁷ The properties of the ISM cloud affect the blockage of the transit signal, in particular, Hydrogen column density, temperature, relative velocity with respect to the star and turbulence.

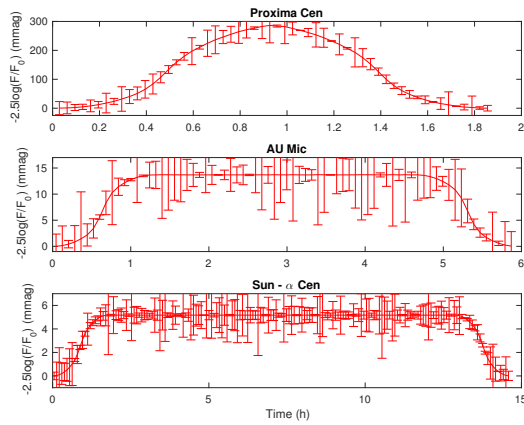


Fig. 6 Observed Ly α light curves (no ISM absorption is considered) according to the noise model and observational configuration described in Sect. 4. SNR(Proxima Cen) = 11.7 obtained with a 4 m telescope and time binning of the photon counts of 2 minutes. SNR(AU Mic) = 3.5 obtained with a 12 m telescope and time binning 4 minutes. SNR(α Cen) = 4.4 obtained with a 12 m telescope and time binning 10 minutes.

observations of exoplanet’s exospheres have only been feasible with the Hubble Space Telescope (HST) orbiting in LEO. However, a similar size telescope but in geosynchronous (or higher) orbit would enjoy a much darker (and stable) Ly α background allowing to carry out efficient Ly α monitoring programs.

WSO-UV is a 170 cm primary mirror space telescope that would be equipped with a solar-blind CsI MCP type detector optimised for the detection of Ly α photons (Shustov et al. 2015a,b, Gómez de Castro et al. 2014). The far UV channel of the camera will be equipped with a prism for slitless spectroscopy providing a resolving power of 800 in the Ly α line to separate cleanly the line from nearby features. As shown in Fig. 7, the sensitivity would be high enough to study the extended distribution of the exospheric hydrogen and measure the impact of stellar activity in Proxima Cen. Moreover, these observations will allow studying the planetary magnetic fields. In the Earth, the scale height of the hydrogen distribution increases with declining solar activity suggesting that the upper thermosphere is not a completely thermalized regime (Qin & Waldrop 2016) and that the energy input from collisions with magnetospheric and solar wind particles cannot be neglected.

However, WSO-UV is far too small to detect Earth-like planets orbiting in the habitable zone around stars bigger than a nearby M5V type star, no to mention around G2V, solar like stars. Therefore, it is worth extending the calculation for the up-coming generation of large space telescopes such as the European Ultraviolet Visible Observatory (EUVO) (Gómez de Castro et al. 2014) or the Large Ultraviolet-Optical-Infrared Observatory (LUVOIR⁸).

⁸ <https://asd.gsfc.nasa.gov/luvoir/>

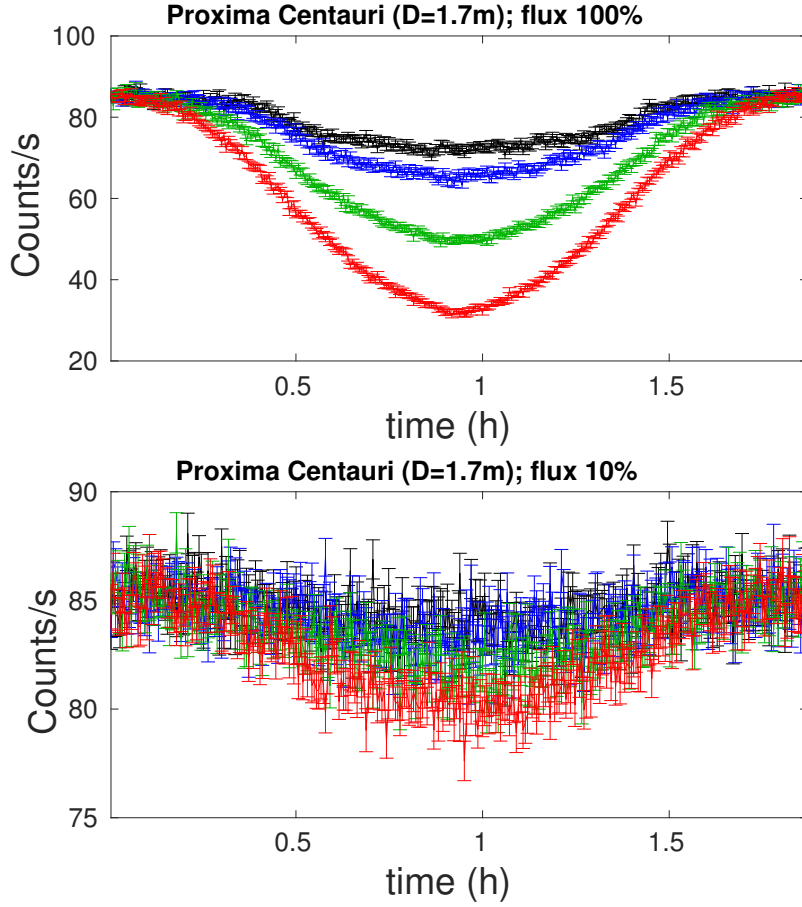


Fig. 7 Impact of the distribution of hydrogen in the exosphere in the transit light curve of Prox Cen as observed by WSO-UV. Models corresponding to $\kappa = 1$ (black), 5 (blue), 10 (green) and 40 (red) are plotted. The light curve has been calculated for the *Case A* and the *Case B* assumptions (0% and 90% of the Ly α flux is absorbed by the ISM, respectively); no temporal binning has been applied and 100 transits have been coadded.

In Figure 8, we have plotted the detectability of transits as a function of the telescope size and the stellar Ly α flux for M type stars. The diagram represents for a given stellar flux, the combination of exposure time and telescope diameter ($\eta = (D/4m)^2 \times T_{exp}$) required to achieve SNR=3 assuming that only a 90% of the transit signature is blocked by local Ly α absorbers. Eq. 9 has been reworked for this purpose to,

$$3 = \left(\frac{\eta A_{eff}}{h\nu_{Ly\alpha}} \right)^{1/2} \frac{\delta F_{Ly\alpha}^*}{F_{Ly\alpha}^*} \left(\frac{F_{Ly\alpha}^*}{1 + 4F_{Back}/F_{Ly\alpha}^*} \right)^{1/2} \quad (13)$$

being $F_{Ly\alpha}^*$ the stellar Ly α flux, $\delta F_{Ly\alpha}^*$ the maximum variation of the Ly α flux during the transit (the depth of the transit in the Ly α light curve, see Figs.4-5) and F_{back} the background Ly α flux. This equation can be transformed into,

$$\eta = \chi \left(\frac{1 + 4F_{Back}/F_{Ly\alpha}^*}{F_{Ly\alpha}^*} \right) \quad (14)$$

with,

$$\chi = 9 \frac{h\nu_{Ly\alpha}}{A_{eff}} \left(\frac{F_{Ly\alpha}^*}{\delta F_{Ly\alpha}^*} \right)^2 \quad (15)$$

a constant that only depends on the depth of the transit, $\delta F_{Ly\alpha}^*/F_{Ly\alpha}^*$. The curves for M5V and M0V stars in Fig. 8 are based on Proxima Centauri and AU Mic light curves (see Fig. 5). T_0 is the exposure time to reach SNR=3 for the Proxima Cen and AU Mic Ly α fluxes (119 s for Proxima Cen and 4 h for AU Mic). For instance, to detect the transit of an Earth-like planet orbiting an M5 star with $F_{Ly\alpha} = 10^{-13}$ erg cm $^{-2}$ s $^{-1}$ requires $\eta/\eta_0 = 40$ that for instance, can be achieved by increasing the size of the primary from 4 to 8 m and co-adding the signal of 10 transits. In a similar manner, it is required $\eta/\eta_0 = 100$ for an M0 star with $F_{Ly\alpha} = 10^{-13}$ erg cm $^{-2}$ s $^{-1}$.

A quick search using the services of the Centre de Données Stellaires (Strasbourg, France) results in 80 stars within 5 pc around the Sun and 47 of them single M-type star. Ly α fluxes have been measured for few of them (Youngblood et al. 2016). There are two M5V stars in the sample, GJ876 and GJ581, and their observed Ly α flux is 0.14×10^{-12} erg s $^{-1}$ cm $^{-2}$ and 0.04×10^{-12} erg s $^{-1}$ cm $^{-2}$. According to Fig. 7, the exosphere of an Earth-like planet would be easily detectable with an 8 m primary space telescope by the transit method.

5 Conclusions

To summarise, it is feasible to measure the distribution of exospheric hydrogen in terrestrial planets orbiting nearby cool M type stars with moderate size (4-8 m primary mirror) space observatories. These measurements are required to understand the dominant processes in the upper atmospheric layers and the energy flow between the atmosphere and the surrounding space because very different levels of space weather conditions can be tested. In this manner, the role of stellar activity and evolutionary state, i.e. the role of particle collisions and planetary magnetic fields in energising the neutral hydrogen atoms, could be addressed rigorously.

References

1. Anglada-Escudé, G., Amado, P.J., Barnes, J. 2016, Nature, 536, 437.
2. Alonso-Floriano, F.J., Morales, J.C., Caballero J. A. et al., A&A, 577,128

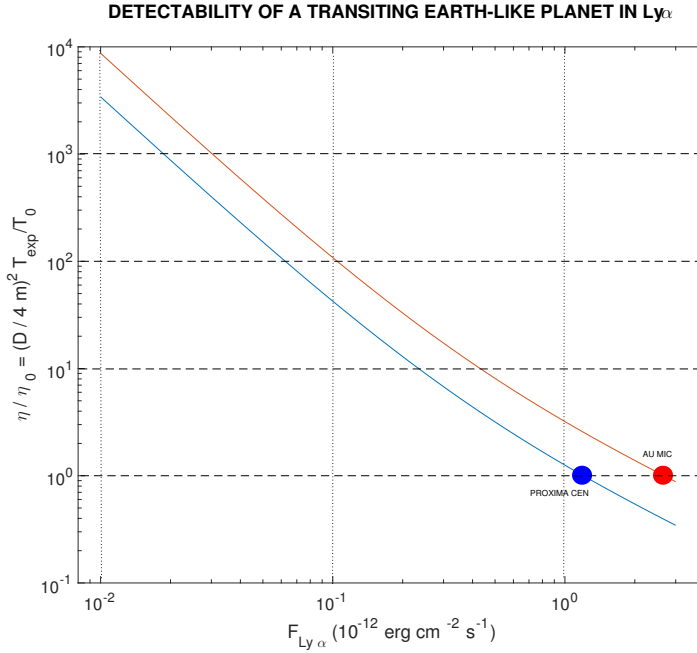


Fig. 8 Detectability of a transiting Earth analogue by flux variations in the Ly α line as a function of the observed Ly α flux (Case B) and the diameter of the primary mirror of the telescope (see text for instrumentation configuration and detectability threshold definition).

3. Berta-Thompson, Z.K., Irwin, J., Charbonneau, D. et al. 2015, *Nature*, 527, 204.
4. Benedict, G. F., Henry, T. J., Franz, O. G., McArthur, B.E., Wasserman, L.H. et al., 2016, *AJ*, 152,5,141
5. Bishop, J. 1999, *J. Quant. Spectrosc. Radiat. Transfer*, 61.
6. Bonfils, X., Gillon, M., Udry, S., Armstrong, D., Bouchy, F. et al 2012, *A&A*, 546, A27.
7. Borucki, W., Koch, D., Basri, G., Batalha, N., Brown, T.M. et al. 2011, *ApJ*, 736, 19.
8. Bourrier, V., Ehrenreich, D., King, G. Lecavelier des Etangs, A., Wheatley, P.J. et al. 2017, *A&A*, 597, 26.
9. Brasseur, G. and Solomon, S. 1996, *Aeronomy of the middle atmosphere. Chemistry and Physics of the Stratosphere and Mesosphere. Atmospheric Science Library*, 5, Springer Ed., ISBN: 978-90-277-2344-4.
10. Chamberlain, J.W. 1963, *Planetary coronae and atmospheric evaporation. Planet. Space Sci.*, 11, 901 (1963).
11. Chen, C. H., Patten, B. M., Werner, M. W., Dowell, C.D., Stapelfeldt, K.R., et al. 2005, *ApJ*, 634, 1372
12. Dessler, A.E., Weinstock, E.M., Hints, E.J., Anderson, J.G., Webster, C.R., et al. 1994, *Geophysical Res. Letters*, 21
13. Dressing, C. D. and Charbonneau, D. 2015, *ApJ*, 807, 45.
14. Ehrenreich, D., Bourrier, V., Bonfils, X., Lecavelier des Etangs, A., Hébrard, G. et al., 2012, *A&A*, 547, 18.
15. Ehrenreich, D., Bourrier, V., Wheatley, P. J., Lecavelier des Etangs, A., Hébrard, G. et al. 2015, *Nature*, 522, 459.
16. Erkaev, N.V., Lammer, H., Odert, P., Kulikov, Y.N., Kislyakova, K.G. et al., 2013, *Astrobiology*, 13, 1011
17. Fuselier, S. A., Burch, J.L., Lewis, W.S., Reiff, P.H. 2000, *Space Science Reviews*, IMAGE special issue, 91, 51.

18. Gómez de Castro, A. I., Belén Perea, G., Sánchez, N., Santiago, J.L., Chirivella, J. et al. 2014, *ApSS*, 354, 177.
19. Gómez de Castro, A.I., Loyd, R.O.P., France, K., Sytov, A., Bisikalo, D., 2016, *ApJL*, 818, L17
20. Koutroumpa, D., Quémerais, E., Katushkina, O., Lallement, R., Bertaux, J.-L. et al., 2017, *A&A*, 598, A12.
21. Kulow, J. R., France, K., Linsky, J., Loyd, R.O.P., 2014, *ApJ*, 786, 132.
22. Lallement, R., Clarke, J.T., Malama, Y., Quémerais, E., Baranov, V.B. et al. 1996. *Science with the Hubble Space Telescope-II*, Space Telescope Institute, P. Benvenuti, F.D. Macchetto, E.J. Schreier, eds.
23. Lecavelier Des Etangs, A., Ehrenreich, D., Vidal-Madjar, A., Ballester, G.E., Désert, J.-M., et al. 2010, *A&A*, 514, 72.
24. Maldonado, J., Affer, L., Micela, G., Scandariato, G., Damasso, M. et al., 2015, *A&A*, 577, 132.
25. McComas, D.J., Allegrini, F., Baldonado, J., Blake, B., Brandt, P.C. et al. 2009, *Space Science Reviews*, 142, 157.
26. Mende, S. B., Heeterks, H., Frey, H. U., Stock, J.M., Lampton, M. et al. 2000. *Space Science Reviews*, 91, 287.
27. Morton, T.D., Bryson, S.T., Coughlin, J.L., Rowe, J.F., Ravichandran, C. et al 2016, *ApJ*, 822, 86.
28. Motalebi, F., Udry, S., Gillon, M., Lovis, C., Ségransan, D., et al., 2015. *A&A*, 584, 72.
29. Østgaard, N., Mende, S.B., Frey, H.U., Gladstone, G.R., Lauche, H., 2003. *Journal of Geophysical Research*, 108, NO. A7, 1300.
30. Pepe, F., Cameron, A.C., Latham, D.W., Molinari, E., Udry, S. et al., 2013. *Nature*, 503, 377-380.
31. Qin, J., Waldrop, L. 2016. *Nature Communications*, 7, 13655.
32. Rairden, R. L., Frank, L. A. , Craven, J. D. 1986. *J. Geophys. Res.* 91, 3613.
33. Redfield, S., Linsky, J.L., *ApJ*, 673, 283
34. Rhee, J.H., Song, I., Zuckerman, B., McElwain, M. 2007, *ApJ*, 660, 1556.
35. Ribas, I., Guinan, E., Güdel, M., Audarc, M., *ApJ*, 62, 680
36. Sachkov, M., Shustov, B., Gómez de Castro, A.I., *Proceedings of the SPIE*, 9905, id.990504
37. Sanz-Forcada, J., Micela, G., Ribas, I., Pollock, A.M.T., Eiroa, C. et al., *A&A*, 53, A6
38. Shizgal, B. D. , Arkos, G. G. 1996. *Rev. Geophys.* 34, 483.
39. Shustov, B.M., Sachkov, M.E., Bisikalo, D., Gómez de Castro, A.-I., 2015, *Characterizing Stellar and Exoplanetary Environments*, *Astrophysics and Space Science Library*, Volume 411. ISBN 978-3-319-09748-0. Springer International Publishing Switzerland, 2015, p. 275
40. Shustov, B., Gomez de Castro, A.I., Sachkov, M., 2015, *Proceedings of the XI Multi-frequency Behaviour of High Energy Cosmic Sources Workshop (MULTIF15)*. 25-30 May 2015. Palermo, Italy.
41. Vallerger, J., McPhate, J., Tremsin, A., Siegmund, O., *ApSS*, 320, 247
42. Vidal-Madjar, A., Lecavelier des Etangs, A., Désert, J.-M., Ballester, G.E., Ferlet, R. et al. 2003, *Nature*, 422, 143.
43. Wood, B.E., Linsky, J.L., Müller, H.-R., Zank, G., 2001. *ApJ*, 547, L49.
44. Wood, B.E., Redfield, S., Linsky, J.L., Müller, H.-R., Zank, G., 2005. *ApJSS*, 159, 118.
45. Youngblood, A., France, K., Loyd, R.O.P., Linsky, J., Redfield, S. et al., 2016, *ApJ*, 824, 101
46. Zoennchen, J. H., Nass, U., Lay, G. & Fahr, H. J. 2010. *Ann. Geophys.* 28, 1221.